Flow analysis and nozzle-shape optimization for the cold-gas dynamic-spray process

M Grujicic[1]*, **W S DeRosset**[2] and **D Helfritch**[2]
[1]Department of Mechanical Engineering, Clemson University, Clemson, South Carolina, USA
[2]Army Research Laboratory, Processing and Properties Branch, Aberdeen, Proving Ground, Maryland, USA

Abstract: An isentropic, one-dimensional model is used to analyse the dynamics of dilute two-phase (feed powder particles plus the carrier gas) flow during the cold-spray process. While the physical foundation of the model is quite straightforward, the solution for the model can be obtained only numerically. The results obtained show that there is a particle-velocity-dependent, carrier-gas-invariant optimal value of the relative gas/particle Mach number that maximizes the drag force acting on feed powder particles and, hence, maximizes the acceleration of the particles. Furthermore, it is found that if the cold-spray nozzle is designed in such a way that at each axial location the acceleration of the particles is maximized, a significant increase in the average velocity of the particles at the nozzle exit can be obtained. For the optimum design of the nozzle, helium as the carrier gas is found to give rise to a substantially higher exit velocity of the particles than air. All these findings are in good agreement with experimental observations.

Keywords: cold-gas dynamic spray process, nozzle design and optimization

NOTATION

A	nozzle cross-sectional area
C	specific heat
C_D	drag coefficient
D	drag force
h	convective heat transfer coefficient
m	mass
$\dot{m}$	mass flowrate
P	pressure
R	gas constant
Re	Reynolds number
S	molecular speed ratio
T	temperature
V	velocity
x	axial distance from the nozzle throat
γ	specific heat ratio
ρ	density

Subscripts

e	exit quantity
P	particle quantity
r	gas/particle relative quantity
s	shock
0	stagnation quantity
∞	freestream quantity

Superscripts

opt	optimal quantity
*	nozzle throat quantity

The MS was received on 26 November 2002 and was accepted after revision for publication on 12 August 2003.
**Corresponding author: Department of Mechanical Engineering, Clemson University, 241 Fluor Daniel Building, Clemson, SC 29634-0921, USA*

1 INTRODUCTION

Thermal spray processes such as high-velocity oxy-fuel, detonation gun, plasma spray and arc spray are widely used to apply protective coatings to parts and to repair worn-out parts (e.g. large-diameter shafts in turbines and pumps). In these processes, the coating material is heated to temperatures high enough to induce melting. Consequently, the high heat input to the part being coated/repaired accompanying these processes can be detrimental if the material of the part degrades when subjected to high temperatures. This problem is generally avoided in the cold-gas dynamic-spray process.

The cold-gas dynamic-spray process, often referred to as simply 'cold spray', is a high-rate material deposition process in which fine, solid powder particles (generally 1−50 μm in diameter) are accelerated in a supersonic

Report Documentation Page

Form Approved
OMB No. 0704-0188

1. REPORT DATE	2. REPORT TYPE	3. DATES COVERED
2003		**00-00-2003 to 00-00-2003**

4. TITLE AND SUBTITLE	5a. CONTRACT NUMBER
Flow analysis and nozzle-shape optimization for the cold-gas dynamic-spray process	5b. GRANT NUMBER
	5c. PROGRAM ELEMENT NUMBER
6. AUTHOR(S)	5d. PROJECT NUMBER
	5e. TASK NUMBER
	5f. WORK UNIT NUMBER
7. PERFORMING ORGANIZATION NAME(S) AND ADDRESS(ES) **Celmson University,Department of Mechanical Engineering,Clemson,SC,29634**	8. PERFORMING ORGANIZATION REPORT NUMBER
9. SPONSORING/MONITORING AGENCY NAME(S) AND ADDRESS(ES)	10. SPONSOR/MONITOR'S ACRONYM(S)
	11. SPONSOR/MONITOR'S REPORT NUMBER(S)

12. DISTRIBUTION/AVAILABILITY STATEMENT
Approved for public release; distribution unlimited

13. SUPPLEMENTARY NOTES

14. ABSTRACT

An isentropic, one-dimensional model is used to analyse the dynamics of dilute two-phase (feed powder particles plus the carrier gas) flow during the cold-spray process. While the physical foundation of the model is quite straightforward, the solution for the model can be obtained only numerically. The results obtained show that there is a particle-velocity-dependent, carrier-gasinvariant optimal value of the relative gas/particle Mach number that maximizes the drag force acting on feed powder particles and, hence, maximizes the acceleration of the particles. Furthermore it is found that if the cold-spray nozzle is designed in such a way that at each axial location the acceleration of the particles is maximized, a significant increase in the average velocity of the particles at the nozzle exit can be obtained. For the optimum design of the nozzle, helium as the carrier gas is found to give rise to a substantially higher exit velocity of the particles than air. All these findings are in good agreement with experimental observations.

15. SUBJECT TERMS

16. SECURITY CLASSIFICATION OF:			17. LIMITATION OF ABSTRACT	18. NUMBER OF PAGES	19a. NAME OF RESPONSIBLE PERSON
a. REPORT	b. ABSTRACT	c. THIS PAGE			
unclassified	**unclassified**	**unclassified**	**Same as Report (SAR)**	**11**	

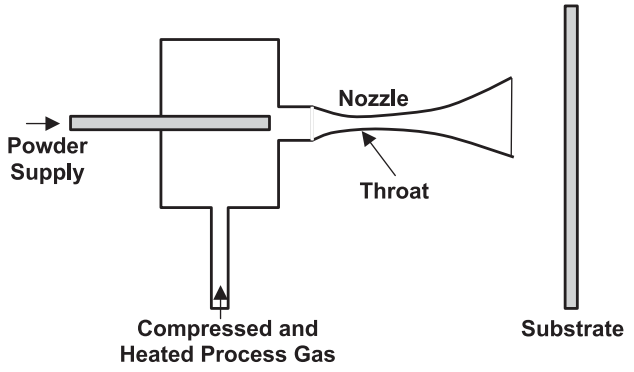

Fig. 1 Schematic of a typical cold-spray system

jet of compressed (carrier) gas to velocities in a range between 500 and 1000 m/s. As the solid particles impact the target surface, they undergo plastic deformation and bond to the surface, rapidly building up a layer of deposited material. Cold spray as a coating technology was initially developed in the mid-1980s at the Institute for Theoretical and Applied Mechanics of the Siberian Division of the Russian Academy of Science in Novosibirsk [**1**, **2**]. The Russian scientists successfully deposited a wide range of pure metals, metallic alloys, polymers and composites on to a variety of substrate materials. In addition, they demonstrated that very high coating deposition rates on the order of 5 m^2/min (~300 ft^2/min) are attainable using the cold-spray process.

A simple schematic of a typical cold-spray device is shown in Fig. 1. Compressed gas of an inlet pressure on the order of 30 bar (500 lb/in^2) enters the device and flows through a converging/diverging nozzle to attain a supersonic velocity. The solid powder particles are metered into the gas flow upstream of the converging section of the nozzle and are accelerated by the rapidly expanding gas. To achieve higher gas flow velocities in the nozzle, the compressed gas is often preheated. However, while preheat temperatures as high as 900 K are sometimes used, due to the fact that the contact time of spray particles with the hot gas is quite short and that the gas rapidly cools as it expands in the diverging section of the nozzle, the temperature of the particles remains substantially below the initial gas preheat temperature and, hence, below the melting temperature of the powder material.

The actual mechanism by which the solid particles deform and bond during cold spray is still not well understood. The prevailing theory for cold-spray bonding postulates that, during impact, the solid particles undergo plastic deformation, disrupt thin (oxide) surface films and, in turn, achieve intimate conformal contact with the target surface. The intimate conformal contact combined with high contact pressures promotes bonding. This theory is supported by a number of experimental findings such as:

1. A wide range of ductile (metallic and polymeric) materials can be successfully cold-sprayed while non-ductile materials such as ceramics can be deposited only if they are co-cold-sprayed with a ductile (matrix) material.
2. The mean deposition particle velocity should exceed a minimum (material-dependent) critical velocity to achieve deposition, which suggests that sufficient kinetic energy must be available to plastically deform the solid material and/or disrupt the surface film.
3. The particle kinetic energy at impact is typically significantly lower than the energy required to melt the particle, suggesting that the deposition mechanism is primarily, or perhaps entirely, a solid-state process. The lack of melting is directly confirmed through micrographic examination of the cold-sprayed materials [**2**].

Because the cold-spray process does not normally involve the use of a high-temperature heat source, it generally offers a number of advantages over the thermal-spray material deposition technologies. Among these advantages, the most important appear to be:

1. The amount of heat delivered to the coated part is relatively small so microstructural changes in the substrate material are minimal or nonexistent.
2. Due to the absence of in-flight oxidation and other chemical reactions, thermally sensitive and oxygen sensitive depositing materials (e.g. copper or titanium) can be cold sprayed without significant material degradation.
3. Nanophase, intermetallic and amorphous materials, which are not amenable to conventional thermal spray processes (due to a major degradation of the depositing material), can be cold sprayed.
4. Formation of the embrittling phases is generally avoided.
5. Macro- and micro-segregations of the alloying elements during solidification that accompany conventional thermal spray techniques and can considerably compromise material properties do not occur during cold spraying. Consequently, attractive properties are retained in cold-sprayed bulk materials.
6. The 'peening' effect of the impinging solid particles can give rise to potentially beneficial compressive residual stresses in cold-spray deposited materials [**3**], in contrast to the highly detrimental tensile residual stresses induced by solidification shrinkage accompanying the conventional thermal-spray processes.
7. Cold spray of materials like copper, solder and polymeric coatings offers exciting new possibilities for cost effective and environmentally friendly alternatives to technologies such as electroplating, soldering and painting [**4**].

The solid state particle-bonding mechanism discussed above suggests and experimental observations (e.g. see reference [**4**]) confirm that it is desirable to maximize the velocity at which feed powder particles impact the

target surface. While, in general, this can be accomplished by increasing the inlet pressure of the carried gas, for practical and economic reasons it is desirable to maximize the particle impact velocity at a given level of the carrier-gas inlet pressure by properly selecting the type of the carrier gas and its inlet temperature and by optimizing the shape of the converging/diverging cold-spray nozzle. A quite detailed analysis of the effect of the type of carrier gas, the gas inlet temperature and the shape of the cold-spray nozzle on the impact velocity of the feed powder particles has been carried out by Dykhuizen and Smith [**5**] using an isentropic, one-dimensional gas-flow model. The objective of the present work is to extend the analysis of Dykhuizen and Smith [**5**] in order to include the effects of the finite particle velocity and variability of the gas/particle drag coefficient.

The organization of the paper is as follows. A brief overview of the one-dimensional isentropic gas flow model developed by Dykhuizen and Smith [**5**] and utilized in this work is presented in section 2. An extension of the particle dynamics model originally proposed by Dykhuizen and Smith [**5**] to include the effect of the finite particle velocity is discussed in section 3. The main results obtained in the present work and pertaining to the determination of an optimum variation of the gas Mach number along the diverging section of the nozzle, optimization of the nozzle shape and the sensitivity of the optimum nozzle shape to variations in the drag coefficient are presented and discussed in sections 4.1, 4.2 and 4.3 respectively. The key conclusions resulting from the present study are summarized in section 5.

2 ISENTROPIC GAS FLOW MODEL

In this section, a brief overview is given of the cold-spray gas-flow model developed by Dykhuizen and Smith [**5**]. The model considers a typical geometry of the cold-spray converging/diverging nozzle (Fig. 1) and involves a number of assumptions and simplifications such as:

1. The gas flow is assumed to be one dimensional and isentropic (adiabatic and frictionless).
2. The gas is treated as a perfect (ideal) gas.
3. The constant-pressure and the constant-volume specific heats of the gas are assumed to be constant.

The carrier gas flow is assumed to originate from a large chamber or duct where its velocity is zero and the pressure (referred to as the 'stagnation' pressure) is P_0 and the temperature (referred to as the 'total' gas temperature) is T_0. The cold-spray process is furthermore assumed to be controlled by the user, who can set the total temperature and the mass flowrate of the gas. The corresponding stagnation pressure can then be calculated using the following procedure.

From the basic dynamic and thermodynamic relations for the compressible fluid flow, the gas temperature T^* at the smallest cross-sectional area of the converging/diverging nozzle (referred to as the 'nozzle throat' in the following) where the Mach number (the velocity of the gas divided by the local speed of sound) is unity can be defined as

$$T^* = \frac{T_0}{1 + (\gamma - 1)/2} \tag{1}$$

where γ is the ratio of the constant-pressure and the constant-volume specific heats and is typically set to 1.66 and 1.4 for monoatomic and diatomic gases respectively. Since air is primarily a mixture of nitrogen and oxygen, it is considered as a diatomic gas. In multi-atom molecular gases, γ takes on values smaller than 1.4, but such gases are rarely used in the cold-spray process.

The gas velocity at the nozzle throat is equal to the speed of sound and is defined as

$$V^* = \sqrt{\gamma R T^*} \tag{2}$$

where R is the gas constant (the universal gas constant divided by the gas molecular weight). It should be noted that the superscript * is used throughout this paper to denote the quantities at the nozzle throat, i.e. the gas quantities under sonic conditions. Equation (2) can be used to explain the experimental finding that the low molecular weight (and, hence, large R), monoatomic (and, hence, large γ and, in turn, high T^*) helium is a better carrier gas than the high molecular weight, diatomic air since for the same total gas temperature, T_0, it is associated with a higher speed of sound.

From the known (user selected) mass flowrate, $\dot{m}$, the sonic gas density can be computed as

$$\rho^* = \frac{\dot{m}}{V^* A^*} \tag{3}$$

where A^* is the (known) cross-sectional area of the nozzle throat. Next, using the ideal gas law, the gas pressure at the nozzle throat can be determined as

$$P^* = \rho^* R T^* \tag{4}$$

Once the throat pressure P^* is computed, the stagnation pressure P_0 can be calculated using the following isentropic relation:

$$P_0 = P^* \left(\frac{T_0}{T^*} \right)^{\gamma/(\gamma-1)} = P^* \left(1 + \frac{\gamma - 1}{2} \right)^{\gamma/(\gamma-1)} \tag{5}$$

After all of the gas-dynamics quantities (T^*, V^*, ρ^* and P^*) have been calculated at the nozzle throat, it is possible to determine these quantities along the diverging section of the nozzle. Towards that end, the variation of one of these quantities or the variation of the Mach number or the variation of the nozzle cross-sectional area along the diverging section of the nozzle must be specified. Dykhuizen and Smith [**5**] considered the case when the variation of the nozzle cross-sectional area A

is specified, which then allows determination of the corresponding Mach number M from the following equation:

$$\frac{A}{A^*} = \left(\frac{1}{M}\right)\left[\left(\frac{2}{\gamma+1}\right)\left(1+\frac{\gamma-1}{2}M^2\right)\right]^{\gamma/[2(\gamma-1)]} \tag{6}$$

Once the Mach number is determined at a given cross-sectional area of the diverging section of the nozzle, the remaining corresponding gas quantities (P, T, V and ρ) can be calculated using the following isentropic relationships:

$$P = P^*\left[\frac{\gamma+1}{2+(\gamma-1)M^2}\right]^{\gamma/(\gamma-1)} \tag{7}$$

$$T = \frac{T_0}{1+[(\gamma-1)/2]M^2} \tag{8}$$

$$V = M\sqrt{\gamma RT} \tag{9}$$

$$\rho = \frac{\rho_0}{\{1+[(\gamma-1)/2]M^2\}^{1/(\gamma-1)}} \tag{10}$$

Equations (7) to (10) can be used to compute P, T, V and ρ at the nozzle exit, if the given exit cross-sectional area A_e is substituted for A in equation (6). However, it must be noted that P, T, V and ρ defined in this way will reflect the true conditions of the gas at the nozzle exit only if normal shock does not take place inside the nozzle. To determine whether the normal shock will take place inside the nozzle, the ambient pressure should be compared with the following 'shock' pressure:

$$P_s = P_e\left(\frac{2\gamma}{\gamma+1}M_e^2 - \frac{\gamma-1}{\gamma+1}\right) \tag{11}$$

where the subscript e is used to denote the gas quantities at the nozzle exit.

If the shock pressure P_s is lower than the ambient pressure, a shock will occur inside the nozzle and the subsequent gas flow is subsonic. Therefore the exit pressure is not given by equation (7) but rather is equal to the ambient pressure. Under normal cold-spray operating conditions, the shock pressure is maintained above the ambient pressure so that no shock occurs inside the nozzle and the exit pressure is defined by equation (7). At the same time, the exit gas pressure, P_e, is generally lower than the ambient pressure in an effort to maximize the exit velocity of the gas (and thus the average velocity of the feed powder particles, referred to as the particle velocity in the following). Under such conditions, the one-dimensional gas dynamics model developed by Dykhuizen and Smith [**5**] and briefly reviewed above can be used to analyse the gas flow inside the nozzle. As the gas leaves the nozzle, it slows down as the gas pressure tries to adjust to the ambient pressure. However, due to a relatively short nozzle exit/target surface standoff distance encountered in the cold-spray process, the decrease in the gas velocity is not expected to be significant and the exit gas velocity can be used as a good approximation of the gas velocity at the target surface.

3 PARTICLE DYNAMICS MODEL

Dykhuizen and Smith [**5**] also analysed the interactions of the carrier gas with the spray particles under the approximation of a dilute two-phase (gas plus non-interacting solid particles) flow. The particle velocity V_P can in this case be determined by solving the following differential equation:

$$m_P\frac{dV_P}{dt} = m_P V_P\frac{dV_P}{dx} = \frac{C_D A_P \rho (V-V_P)^2}{2} \tag{12}$$

where m_P and A_P are the average mass and cross-sectional area of the particles respectively, C_D is the drag coefficient, t the time and x the axial distance travelled by the particle (measured from the nozzle throat). Equation (12) shows that the maximum particle velocity is equal to the gas velocity. Under the condition of constant gas velocity, gas density and drag coefficient, equation (12) can be integrated to yield

$$\log\left(\frac{V-V_P}{V}\right) + \frac{V}{V-V_P} - 1 = \frac{C_D A_P \rho x}{2m_P} \tag{13}$$

When the particle velocity is very small in comparison to the gas velocity, equation (13) can be simplified as

$$V_P = V\sqrt{\frac{C_D A_P \rho x}{m_P}} = V\sqrt{\frac{3C_D \rho x}{2D_P \rho_P}} \tag{14}$$

which is consistent with experimental observations [6] that the spray particle velocity is proportional to the square root of the ratio of the distance travelled x and the particle diameter D_P. In equation (14) ρ_P denotes the particle material density.

A simple analysis of equation (12) shows that the ultimate particle velocity is equal to the gas velocity. Furthermore, examination of equations (6), (8) and (9) indicates that the gas velocity within the nozzle depends on the total gas temperature and the nozzle geometry (i.e. the cross-sectional area at a given axial distance x) but not on the gas pressure. However, equations (9), (10) and (12) indicate that the initial particle acceleration (dV_P/dt at $V_P = 0$) is linearly dependent on the stagnation pressure but independent of the total temperature. Thus, while the stagnation pressure does not affect the maximum particle velocity, it has to be sufficiently high to ensure that the spray particle velocity will approach the gas velocity over a relatively short length of the diverging section of the nozzle.

4 RESULTS AND DISCUSSION

4.1 Determination of the optimum Mach number

Equation (12) shows that the particle acceleration, dV_P/dt, is influenced by two quantities of the carrier gas: the gas velocity and the gas density. Since these two conditions are mutually coupled through the gas dynamics equations (and, consequently, the gas density decreases as the gas velocity increases along the diverging section of the nozzle), an optimal condition of the gas exists that maximizes the particle acceleration. This condition corresponds to the maximum of the drag force acting on the particle [the right-hand side of equation (12)]. Under the assumption that the particle velocity is small in comparison to the gas velocity (i.e. $V_P \ll V$) and for constant C_D, the optimal gas condition can be obtained by differentiating the drag force, D (the right-hand side of equation (12) with $V_P = 0$), with respect to the Mach number to yield

$$\frac{dD}{dM} = \frac{C_D A_P M}{2}\left(1 + \frac{\gamma - 1}{2} M^2\right)^{-\gamma/(\gamma-1)} \times \frac{2 - M^2}{1 + [(\gamma - 1)/2] M^2} \tag{15}$$

Since $\gamma > 1$, equation (15) shows that the maximum acceleration of a stationary particle is achieved at the gas velocity of Mach $\sqrt{2}$ at which $dD/dM = 0$.

The optimum value of the gas Mach number (or the relative Mach number defined as a difference between the gas and the particle Mach numbers) at different values of the particle velocity (or the particle Mach number $M_P = V_P/\sqrt{\gamma RT}$) are determined in the present work, by finding (numerically) the maximum in the drag force, D, in which the V^2 term is replaced by a $(V - V_P)^2$ term. The results of this calculation are presented in Fig. 2.

Figures 2a and b show the drag force (normalized by $2/(C_D A_P)$ contour plots as a function of the particle Mach number with respect to T^*, $M_P^* = V_P/\sqrt{\gamma RT^*}$) and the relative gas Mach number $M_r = (V - V_P)/\sqrt{\gamma RT}$ for air and helium as the carrier gases. The following (typical) cold-spray processing conditions are used to generate the results presented in Figs 2a and b, as well as throughout the rest of this paper: the total gas temperature $T_0 = 600\,\mathrm{K}$, the stagnation pressure $P_0 = 22\,\mathrm{bar}$, the mean particle diameter $D_P = 10\,\mu\mathrm{m}$ and the particle material density $\rho_P = 8\,\mathrm{g/cm^3}$.

The results presented in Figs 2a and b show that, for both air and helium, the maximum drag force occurs at a relative Mach number (referred to as the optimum relative Mach number, M_r^{opt}) whose value decreases with an increase in the particle Mach number (i.e. with the particle velocity). The variation of the optimum relative Mach number with respect to the particle Mach number M_P^* is shown in Fig. 2c. It is seen that the decrease in the optimum relative Mach number with an increase in the particle Mach number is somewhat more pronounced in helium than in air. The variation of the optimum relative Mach number with respect to the particle Mach number relative to the actual gas temperature T, $M_P = V_P/\sqrt{\gamma RT}$, is shown in Fig. 2d. It is seen that, as expected, the optimum relative Mach number decreases with an increase in the particle Mach number. Furthermore, it is seen that the M_r^{opt} versus M_P relationship is independent of the type of carrier gas. The results presented in Figs 2c and d are generally consistent with experimental findings, which show that the spray particle velocity is maximal at a Mach number around unity [6].

4.2 Optimization of the nozzle shape

The analysis presented in the previous section indicates that in order to maximize the spray particle acceleration at each axial location along the diverging section of the nozzle, the relative Mach number should take on a value equal to the value of the optimal relative Mach number corresponding to the local value of the particle Mach number. Dykhuizen and Smith [**5**] assumed that the optimal value of the relative Mach number is independent of the particle Mach number and that it is equal to unity. Instead, in the present paper, the optimal value of the relative Mach number is taken to be defined by the M_r^{opt} versus M_P relationship, as displayed in Fig. 2d. The relationship between the gas and the particle velocities can then be expressed as

$$V - V_P = M_r^{opt}\sqrt{\gamma RT} \tag{16}$$

In this section, a procedure for optimization of the nozzle shape which maximizes the exit particle velocity for the given gas stagnation pressure, the total gas temperature and the spray particle properties is presented. Differentiation of equation (16) with respect to the axial position of the particle yields

$$\frac{dV}{dx} - \frac{dV_P}{dx} = M_r^{opt}\frac{\sqrt{\gamma RT}}{2T}\frac{dT}{dx} + \frac{dM_r^{opt}}{dM_P}\frac{dM_P}{dV_P}\frac{dV_P}{dx}\sqrt{\gamma RT} \tag{17}$$

Differentiation of equation (9) gives

$$\frac{dV}{dx} = \sqrt{\gamma RT}\frac{dM}{dx} + \frac{M\sqrt{\gamma RT}}{2T}\frac{dT}{dx} \tag{18}$$

while combining equations (12) and (16) and differentiating with respect to x gives

$$\frac{dV_P}{dx} = \frac{\sqrt{\gamma RT} C_D A_P \rho}{2 m_P (M - M_r^{opt})} \tag{19}$$

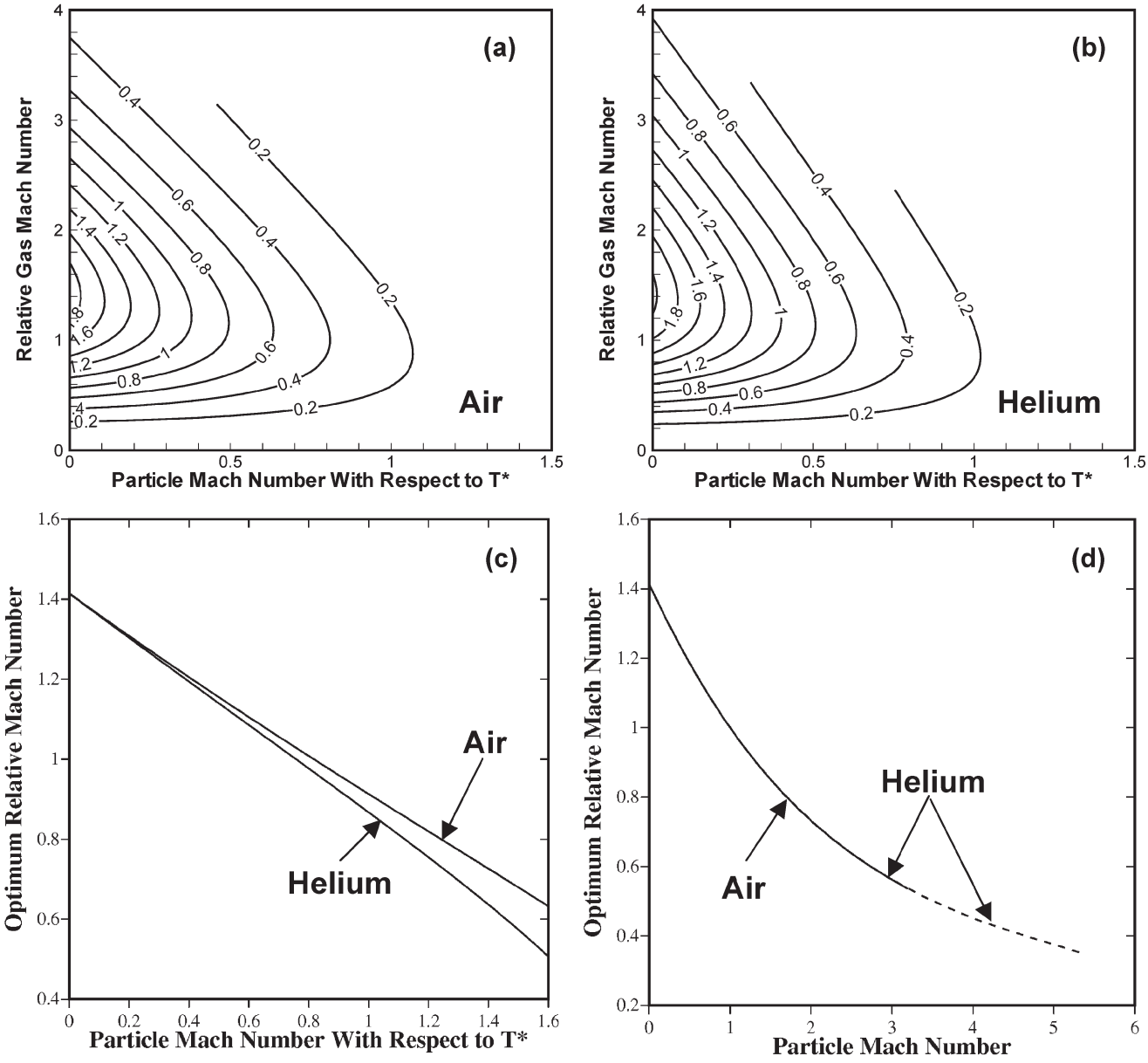

Fig. 2 (a) and (b) Contour plots of the normalized drag force relative to variations in the particle Mach number and the relative gas Mach number for air and helium as the carrier gases. (c) and (d) Variations of the optimum relative gas Mach number with respect to the particle Mach number relative to the nozzle throat temperature T^* and the actual gas temperature T respectively

Also, differentiation of equation (8) gives

$$\frac{\mathrm{d}T}{\mathrm{d}x} = \frac{2T_0}{2+(\gamma-1)M^2} \tag{20}$$

Combining equations (17) to (20) and using equation (10) gives

$$\frac{\mathrm{d}M}{\mathrm{d}X}\left[\frac{2+(\gamma-1)MM_{\mathrm{r}}^{\mathrm{opt}}}{2+(\gamma-1)M^2}\right](M-M_{\mathrm{r}}^{\mathrm{opt}}) = \left[\frac{2+(\gamma-1)M^2}{2}\right]^{-1/(\gamma-1)}(M_{\mathrm{r}}^{\mathrm{opt}})^2\left(1+\frac{\mathrm{d}M_{\mathrm{r}}^{\mathrm{opt}}}{\mathrm{d}M_{\mathrm{P}}}\right) \tag{21}$$

where

$$X = \frac{xC_{\mathrm{D}}A_{\mathrm{P}}\rho_0}{2m_{\mathrm{P}}} \tag{22}$$

and the stagnation density, ρ_0, is defined by the ideal gas law as

$$\rho_0 = \frac{P_0}{RT_0} \tag{23}$$

The optimal variation of the Mach number along the length of the diverging section of the nozzle is obtained by solving equation (21). It should be noted that, since the normalized axial variable X depends on

the stagnation density ρ_0 [and via equation (23) on the stagnation pressure P_0, the total gas temperature T_0 and the gas molecular weight], the optimal variation of the Mach number, $M(x)$, and, via equation (6), the optimal variation in the nozzle cross-section expansion ratio, A/A^*, along the diverging section of the nozzle are influenced by the cold-spray processing (stagnation) conditions and by the type of carrier gas used. Once the optimal variation of the Mach number is found, the corresponding variation of the particle velocity is obtained by combining equations (8), (9) and (10) to get

$$V_P = (M - M_r^{opt})\sqrt{\frac{\gamma R T_0}{1 + [(\gamma - 1)/2]M^2}} \tag{24}$$

As discussed earlier, due to a short standoff distance encountered in the cold-spray process, the effect of particle deceleration upon exiting the nozzle is not expected to be significant. Hence, if equation (24) is used to compute the particle velocity at the nozzle exit, such velocity is expected to be a good approximation for the velocity at which the feed powder particles impact the target surface.

As pointed out earlier, the axial position (X) in equation (21) is measured from the nozzle throat, so by solving this equation and using equation (6) the optimal shape (i.e. the optimal expansion ratio profile, A/A^*) of the diverging section of the nozzle is obtained. The converging section of the nozzle, on the other hand, is desirable to be as short as possible in order to attain the required Mach 1 gas velocity at the nozzle throat quickly. However, for the isentropic flow conditions used in the model to be satisfied, a gradually converging section of the nozzle is required.

Equation (21) is solved numerically in the present work using a first-order, forward difference scheme. All the calculations are carried out for a 0.1 m long diverging section of the cold-spray nozzle and under the condition of a constant drag coefficient C_D whose value is set to 1. The remaining cold-spray processing and feed powder conditions are set identical to the ones used in the previous section: the total gas temperature $T_0 = 600\,\text{K}$, the stagnation pressure $P_0 = 22\,\text{bar}$, the mean particle diameter $D_P = 10\,\mu\text{m}$ and the particle material density $\rho_P = 8\,\text{g/cm}^3$. Once the optimal variation of the Mach number along the diverging section of the nozzle is determined, equation (24) is used to obtain the corresponding variation of the gas velocity. Next, equation (12) is used to calculate the corresponding variation of the particle velocity and, finally, equation (6) is used to determine the optimal nozzle shape (i.e. the optimal variation of the optimal nozzle cross-section expansion ratio). The results of this calculation are presented in Fig. 3. For comparison, the corresponding results obtained under the approximation used by Dykhuizen and Smith [**5**], that the optimal relative Mach number is 1, are also presented.

The results displayed in Fig. 3a show the variation of the velocity of air and helium along the diverging section of the nozzle. The corresponding results obtained under the assumption used by Dykhuizen and Smith [**5**] are denoted as 'Ref. [5]' in Fig. 3a, as well as in the subsequent figures. The results shown in Fig. 3a indicate that by setting the relative Mach number to its optimal value at each axial location along the diverging section of the nozzle, the gas exit velocity can be increased by ~5.3 per cent for air and by ~2.6 per cent for helium relative to the ones obtained under the condition of a relative Mach 1 number.

The variation of the particle velocity along the diverging section of the nozzle for the cases of air and helium as the carrier gases is displayed in Fig. 3b. The results shown in Fig. 3b indicate that by setting the relative Mach number to its optimal value at each axial location along the diverging section of the nozzle, the gas particle velocity can be increased by ~3.5 per cent for air and by ~17 per cent for helium as the carrier gas relative to the particle velocities obtained under the condition of a relative Mach 1 number. The significantly smaller increase in the particle velocity for the case of air as the carrier gas can be understood by comparing the results shown in Figs 3a and b. It is seen that, in the case of air, the particle velocity is already within 5 per cent of the air velocity under the condition of a relative Mach 1 number.

The variation of the optimal nozzle cross-section expansion ratios along the diverging section of the nozzle for helium and air as the carrier gases is shown in Fig. 3c. It is seen that the optimal nozzle cross-section expansion ratios for helium and air as the carrier gases are quite different from their counterparts obtained under the approximation used by Dykhuizen and Smith [**5**].

The variation of the gas pressure and the corresponding shock pressure along the diverging section of the nozzle for helium and air as the carrier gases is shown in Fig. 3d. In addition, the ambient pressure of 1 atm is also indicated in the same figure. It is seen that the shock pressure for both air and helium remains above the ambient pressure until the nozzle exit, suggesting that the normal shock will not occur within the cold-spray nozzle. Furthermore, it is seen that in the case of air, the gas flow is overexpanded, i.e. the air exit pressure is lower than the ambient pressure. As discussed earlier, this scenario is typically encountered in the cold-spray process.

The results shown in Fig. 3d further indicate that there is a maximum allowable, carrier-gas dependent length of the diverging section of the nozzle which, if exceeded, would give rise to the occurrence of the normal shock inside the nozzle. If longer nozzles are needed under specific circumstances, they may be allowed, but the

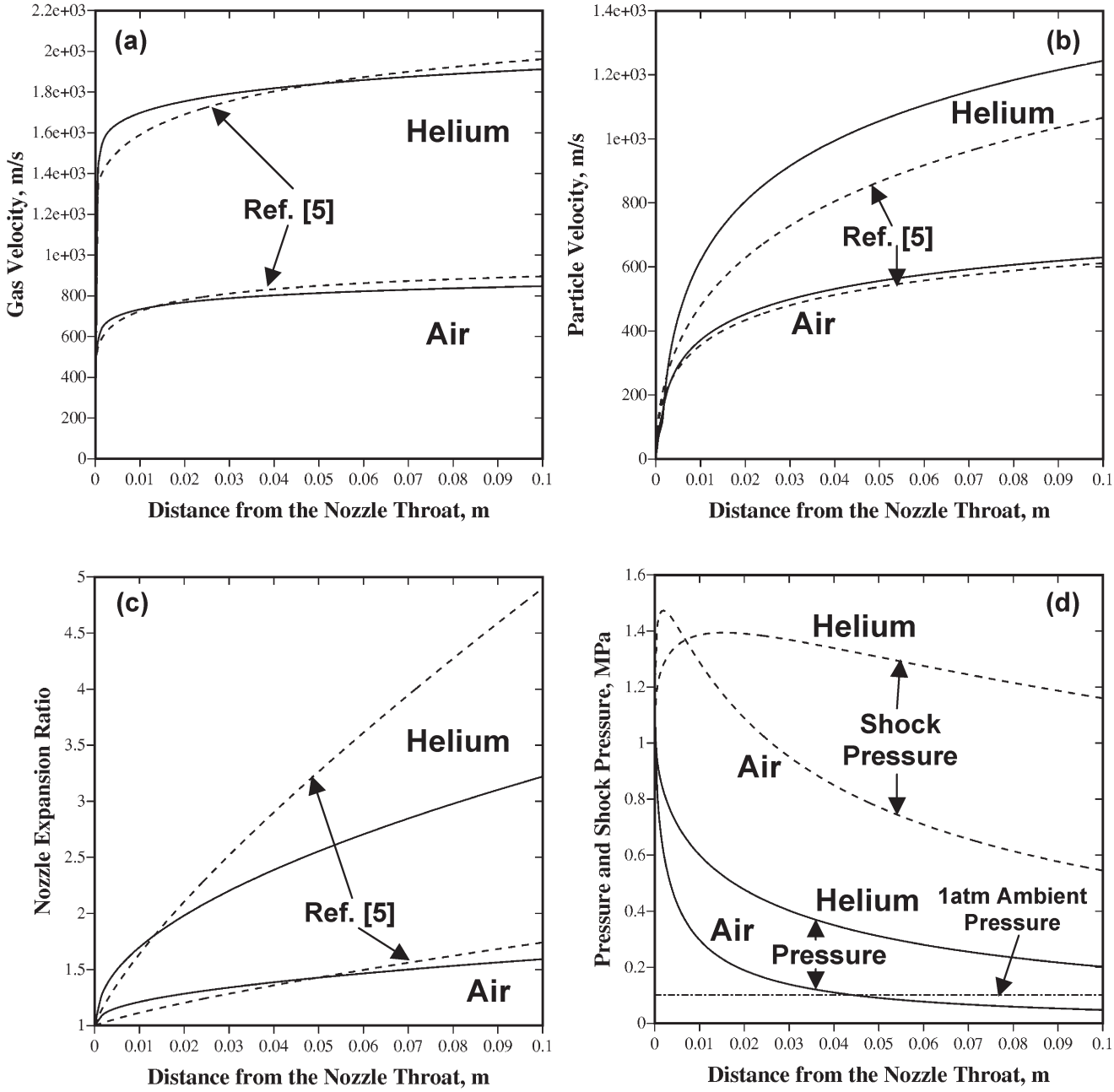

Fig. 3 Variations of (a) the gas velocity, (b) the particle velocity, (c) the optimum nozzle cross-section expansion ratio and (d) the pressure and the shock pressure along the diverging section of the nozzle under a constant drag coefficient, $C_D = 1$. See the text for details of the cold-spray processing conditions and feed powder properties

nozzle cross-sectional area must remain constant after the maximum allowable value of the expansion ratio is reached in order to prevent the normal shock from occurring inside the nozzle.

4.3 Effect of the variable drag coefficient

All the calculations performed in the previous sections were carried out under the condition that the drag coefficient C_D is constant and equal to unity. In this section, the effect of variation in the magnitude of the drag coefficient with the flow conditions on the particle exit velocity and on the optimal variation in the nozzle cross-section expansion ratio is analysed.

The drag coefficient correlating equations for spherical particles over a wide range of flow conditions as developed by Henderson [7] are used in the present work. For the subsonic flow, Henderson [7] proposed

the following relation:

$$C_D = 24\left\{ Re + S\left[4.33 + \left(\frac{3.65 - 1.53T_P/T}{1 + 0.353T_P/T}\right) \times \exp\left(-0.247\,\frac{Re}{S}\right)\right]\right\}^{-1} + \exp\left(-\frac{0.5M_r}{\sqrt{Re}}\right)\left[\frac{4.5 + 0.38(0.03Re + 0.48\sqrt{Re})}{1 + 0.03Re + 0.48\sqrt{Re}} + 0.1M_r^2 + 0.2M_r^8\right] + \left[1 - \exp\left(-\frac{M_r}{Re}\right)\right]0.6S \quad (25)$$

where $Re = \rho\,\Delta v\,D_P/\mu$ is the Reynolds number based on the particle diameter, D_P, the relative gas/particle velocity, Δv, the freestream gas density, ρ, and viscosity, μ. M_r is the relative Mach number and $S = M_r\sqrt{\gamma/2}$. T_P in equation (25) denotes the (uniform) particle temperature and T the freestream gas temperature.

For the supersonic regime at Mach numbers equal to or exceeding 1.75, Henderson [7] proposed the following expression:

$$C_D = \frac{0.9 + \dfrac{0.34}{M_\infty^2} + 1.86\left(\dfrac{M_\infty}{Re_\infty}\right)^{1/2} \times \left[2 + \dfrac{2}{S_\infty^2} + \dfrac{1.058}{S_\infty}\left(\dfrac{T_P}{T}\right)^{1/2} - \dfrac{1}{S_\infty^4}\right]}{1 + 1.86\left(\dfrac{M_\infty}{Re_\infty}\right)^{1/2}} \quad (26)$$

where the subscript ∞ is used to denote the freestream quantities. For the supersonic regime at Mach numbers between 1.0 and 1.75, Henderson [7] proposed the following linear interpolation:

$$C_D(M_\infty, Re_\infty) = C_D(1.0, Re) + \tfrac{4}{3}(M_\infty - 1.0) \times [C_D(1.75, Re_\infty) - C_D(1.0, Re_\infty)] \quad (27)$$

where $C_D(1.0, Re)$ denotes the drag coefficient calculated using equation (25) at $M_r = 1.0$ and $C_D(1.75, Re_\infty)$ represents the drag coefficient calculated using equation (26) with $M_\infty = 1.75$.

To include the effect of variability of the drag coefficient on the particle exit velocity and on the optimal shape of the diverging section of the cold-spray nozzle, equation (21) is solved numerically while the drag coefficient C_D at each axial location of the nozzle is assigned a value consistent with the local flow conditions, as defined by the appropriate correlating equation [equation (25), (26) or (27)]. The results of this calculation are shown in Figs 4 and 5.

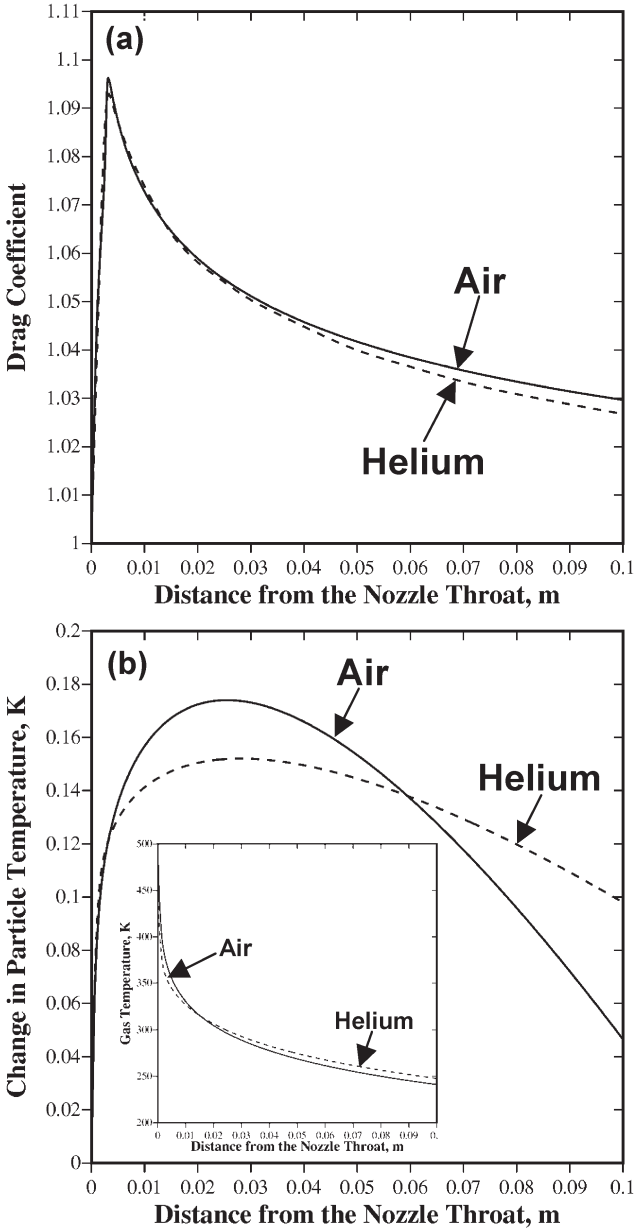

Fig. 4 Variations of (a) the drag coefficient and (b) the change in the particle temperature (and gas temperature; see the inset) along the length of the diverging section of the nozzle

The variation of the drag coefficient in the case of a nozzle with a throat diameter of 0.01 m along the length of the diverging section of the nozzle for air and helium as the carrier gases is shown in Fig. 4a. The variation of the (uniform) particle temperature, T_P, along the length of the diverging section of the nozzle [used for calculation of the drag coefficient in equations (25) to (27)] is obtained by numerically integrating the following heat conservation equation:

$$m_P C_P\,dT_P = A_P h(T - T_P)\,dt = A_P h(T - T_P)\,\frac{dx}{V_P} \quad (28)$$

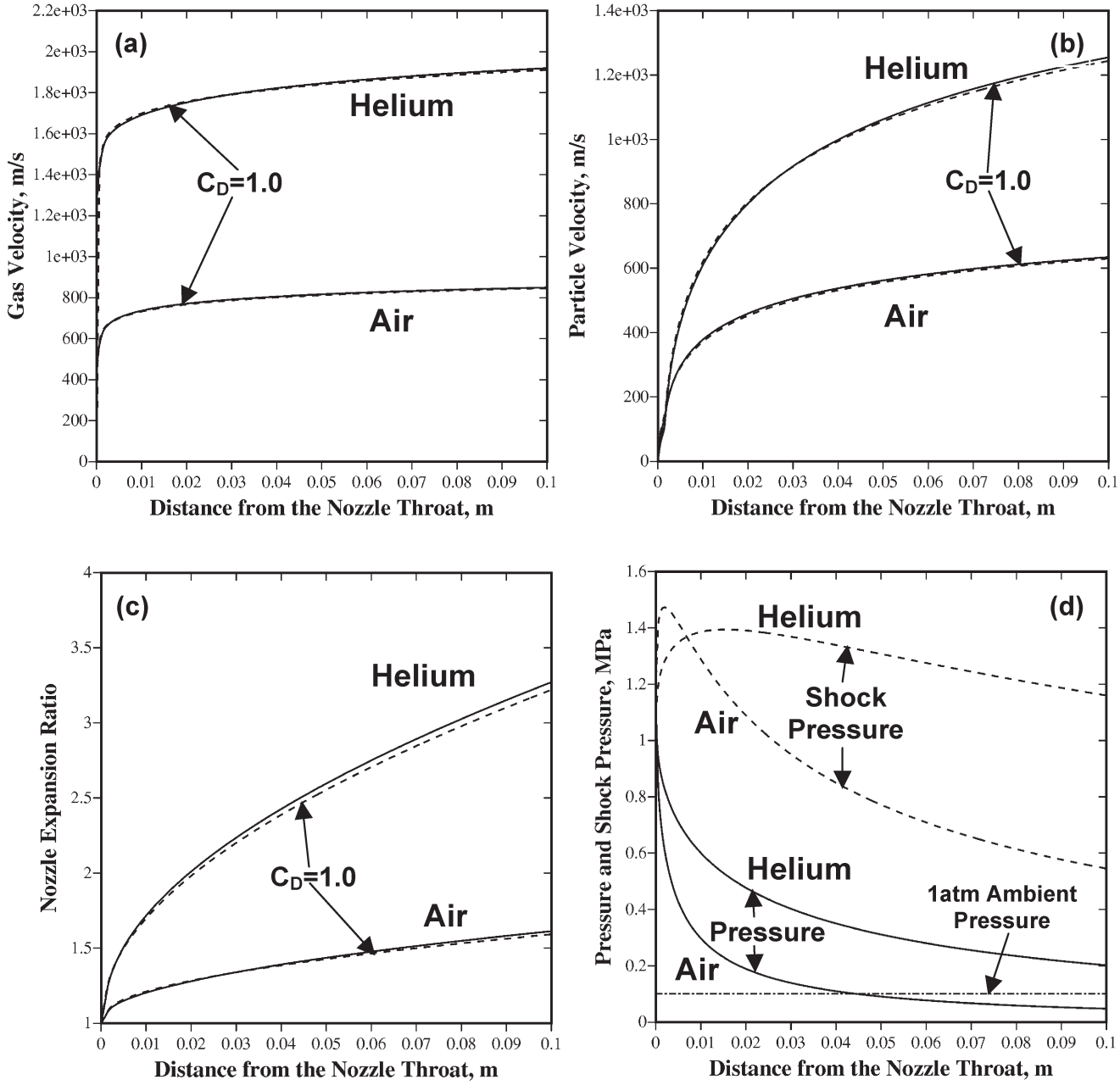

Fig. 5 Variations of (a) the gas velocity, (b) the particle velocity, (c) the optimum nozzle cross-section expansion ratio and (d) the pressure and the shock pressure along the diverging section of the nozzle under a variable and a constant ($C_D = 1$) drag coefficient

with $T_P(x = 0) = 295\,K$ and where the specific heat, $C_P(= 460\,J/kg\,K)$, is set to the value common for austenitic stainless steels. The convective heat transfer coefficient, h, on the other hand, is assigned a typical natural convection value of $190\,W/m^2\,K$. It should be noted that, depending of the flow conditions inside the cold-spray nozzle, the value of the convective heat transfer coefficient can be significantly higher than the value used. The effect of the magnitude of the convective heat transfer coefficient is not, however, studied in the present work.

The results displayed in Fig. 4a show that for both air and helium, the drag coefficient takes on values that exceed one. Consequently, the drag force and, hence, the particle exit velocities are expected to be larger than the ones obtained under the $C_D = 1$ condition. An abrupt change in the drag coefficient seen in Fig. 4a is associated with the sudden change in relative Mach number, which initially increases from its value of one at the nozzle throat and, after it reaches the optimal value, starts to decrease as the optimal value of the relative Mach number decreases with the increasing particle Mach number (Figs 2c and d).

The results displayed in Fig. 4b show that the particle temperature changes by less than 0.2 K relative to the initial particle temperature (295 K) for both air and

helium as the carrier gases. Initially, as seen in the inset of Fig. 4b, the carrier gas has a higher temperature than the particles and, consequently, the particle temperature rises. However, as the carrier gas rapidly expands downstream in the diverging section of the nozzle, its temperature decreases below the particle temperature, causing the particle temperature to begin to decrease. In any case, the average particle resident time $\int_0^l \mathrm{d}x/V_\mathrm{P}$ ($l = 0.1\,\mathrm{m}$ is the length of the nozzle) is quite short ($\sim$0.2 ms for air and $\sim$0.1 ms for helium) so the overall change in the particle temperature is quite small. It should be noted that the magnitude of the particle temperature change is greatly affected by the choice of the convective heat transfer coefficient, h.

The variations of the gas velocity, the particle velocity, the optimal nozzle cross-section expansion ratio and the pressure/shock pressure along the diverging section of the nozzle are shown in Figs 5a to d respectively. For comparison, the variations in the same quantities under the $C_\mathrm{D} = 1$ condition are displayed in Figs 5a to c and denoted using dashed lines and a '$C_\mathrm{D} = 1$' label.

The results displayed in Figs 5a to c show that the variability of the drag coefficient has a relatively small effect on the variation of the gas velocity, the particle velocity and the optimal shape of the diverging section of the cold-spray nozzle. This finding is consistent with the results displayed in Fig. 4a which show that, while the drag coefficient varies along the length of the diverging section of the nozzle, its value never departs more than 10 per cent from $C_\mathrm{D} = 1.0$. As predicted, since C_D takes on values larger than 1, the particle velocities are larger than the ones obtained under the $C_\mathrm{D} = 1.0$ condition. However, this effect is relatively small. The results displayed in Fig. 5d show that the inclusion of the dependence of the drag coefficient on the flow conditions does not cause normal shock to occur inside the nozzle and that the air flow is again overexpanded.

5 CONCLUSIONS

Based on the results obtained in the present work, the following main conclusions can be drawn:

1. Due to its monoatomic character and a lower molecular weight, helium is a more efficient carrier gas, giving rise to roughly twice the average particle exit velocity as that obtained in the case of air as the carrier gas under the otherwise identical cold-spray processing conditions.
2. For the given cold-spray processing conditions and a fixed particle size, the average exit particle velocity can be significantly increased by ensuring (via the use of a properly designed nozzle) that the gas/particle relative Mach number takes on a particle-velocity-dependent, carrier-gas-invariant optimal value.
3. For both air and helium as the carrier gases, the gas/particle drag coefficient C_D under the typical cold-spray processing conditions does not depart significantly from unity. Consequently, the frequently used $C_\mathrm{D} = 1$ simplification appears justified.

ACKNOWLEDGEMENTS

The material presented in this paper is based on work supported by the US Army Grant DAAD19-01-1-0661. The authors are indebted to Drs Walter Roy and Fred Stanton of the ARL for their support and a continuing interest in the present work. The authors also acknowledge the support of the Office of High Performance Computing Facilities at Clemson University.

REFERENCES

1 **Alkhimov, A. P., Papyrin, A. N., Dosarev, V. F., Nestorovich, N. I.** and **Shuspanov, M. M.** Gas dynamic spraying method for applying a coating. US Pat. 5,302,414, 12 April 1994.
2 **Tokarev, A. O.** Structure of aluminum powder coatings prepared by cold gas dynamic spraying. *Metal Sci., Heat. Treat.*, 1996, **35**(3–4), 136–139.
3 **McCune, R. C., Papyrin, A. N., Hall, J. N., Riggs, W. L.** and **Zajchowski, P. H.** An exploration of the cold gas–dynamic spray method for several material systems. In *Thermal Spray Science and Technology* (Eds C. C. Berndt and S. Sampath), 1995, pp. 1–5 (ASM International, Ohio).
4 **Bishop, C. V.** and **Loar, G. W.** Practical pollution abatement method for metal finishing. *Plate Surf. Finish*, 1993, **80**(2), 37–39.
5 **Dykhuizen, R. C.** and **Smith, M. F.** Gas dynamic principles of cold spray. *J. Therm. Spray Technol.*, 1998, **7**(2), 205–212.
6 **Neiser, R. A., Brodeman, J. E., Ohern, T. J., Smith, M. F., Dykhuizen, R. C., Roemer, T. J.** and **Teets, R. E.** Wire melting and droplet atomization in a high velocity oxy-fuel jet. In *Thermal Spray Science and Technology* (Eds C. C. Berndt and S. Sampath), 1995, pp. 99–104 (ASM International, Ohio).
7 **Henderson, C. B.** Drag coefficients of spheres in continuum and rarefied flows. *Am. Inst. Aeronaut. Astronaut. J.*, 1976, **14**(1), 707–708.